A blurred reflection interpretation for the intermediate flux state in Mrk 335

L. C. Gallo,[1]★ A. C. Fabian,[2] D. Grupe,[3] K. Bonson,[1] S. Komossa,[4]
A. L. Longinotti,[5] G. Miniutti,[6] D. J. Walton,[2,7] A. Zoghbi[8] and S. Mathur[9]

[1]*Department of Astronomy and Physics, Saint Mary's University, 923 Robie Street, Halifax, NS B3H 3C3, Canada*
[2]*Institute of Astronomy, University of Cambridge, Madingley Road, Cambridge CB3 0HA*
[3]*Department of Astronomy and Astrophysics, Pennsylvania State University, 525 Davey Lab, University Park, PA 16802, USA*
[4]*Max-Planck-Institut für Radioastronomie, Auf dem Hügel 69, 53121 Bonn, Germany*
[5]*XMM-Newton Science Operations Centre, ESA, Villafranca del Castillo, Apartado 78, E-28691 Villanueva de la Cañada, Spain*
[6]*Centro de Astrobiologia (CSIC-INTA), Dep. de Astrofisica; LAEFF, PO Box 78, E-28691 Villanueva de la Cañada, Madrid, Spain*
[7]*California Institute of Technology, 1200 East California Boulevard, Pasadena, CA 91125, USA*
[8]*Department of Astronomy, University of Maryland, College Park, MD 20742, USA*
[9]*Astronomy Department, The Ohio State University, Columbus, OH 43210, USA*

ABSTRACT

As part of a long-term monitoring campaign of Mrk 335, deep *XMM–Newton* observations catch the narrow-line Seyfert 1 galaxy (NLS1) in a complex, intermediate flux interval as the active galaxy is transiting from low to high flux. Other works on these same data examined the general behaviour of the NLS1 and the conditions of its warm absorber. The analysis presented here demonstrates the X-ray continuum and timing properties can be described in a self-consistent manner adopting a blurred reflection model without any need to invoke partial covering. The rapid spectral variability appears to be driven by changes in the shape of the primary emitter that is illuminating the inner accretion disc around a rapidly spinning black hole ($a > 0.7$). While light bending is certainly prominent, the rather constant emissivity profile and break radius obtained in our spectral fitting suggest that the blurring parameters do not change as would be expected if the primary source varies its distance from the disc. Instead changes could be intrinsic to the power-law component. One possibility is that material in an unresolved jet above the disc falls to combine with material at the base of the jet producing the changes in the primary emitter (spectral slope and flux) without changing its distance from the disc.

Key words: galaxies: active – galaxies: individual: Mrk 335 – X-ray: galaxies – galaxies: nuclei.

1 INTRODUCTION

The narrow-line Seyfert 1 galaxy (NLS1), Mrk 335 ($z = 0.025785$), has always been the subject of intense scrutiny. As one of the brighter active galactic nuclei (AGNs) in the X-ray sky it has been observed by most major missions so its long-term behaviour is relatively well established (Grupe et al. 2008). Its X-ray continuum has normally been described with a power law and soft excess (e.g. Pounds et al. 1987). More sensitive observations revealed a narrow emission line around 6.4 keV along with a broader emission feature in the Fe Kα region. The combination of the soft excess and broad emission feature is indicative of reflection from the inner region of

an ionized disc (e.g. Ross & Fabian 2005) and such models have been successful in fitting the spectra of Mrk 335 (e.g. Ballantyne, Iwasawa & Fabian 2001; Crummy et al. 2006; O'Neill et al. 2007; Larsson et al. 2008; Longinotti et al. 2008).

A 2007 *Swift* snap-shot of Mrk 335 found the NLS1 in an unprecedented low state where the X-ray flux had diminished to about 1/30 of the previously lowest observed flux state (Grupe, Komossa & Gallo 2007). The *Swift* observation showed considerable curvature in the X-ray spectrum, and simultaneous optical data found that the AGN was in an X-ray weak state. Both factors are indicative of either absorption or reflection dominating the spectrum (Gallo 2006). The *Swift* observation prompted a 20 ks *XMM–Newton* Target of Opportunity observation that revealed low-energy emission lines from a photoionized gas likely originating far from the inner accretion disc and close to the broad line region (Grupe et al. 2008;

★ E-mail: lgallo@ap.smu.ca

Longinotti et al. 2008). During this low state the continuum could be described equally well as arising from either partial covering or blurred reflection (Grupe et al. 2008).

Since 2007 Mrk 335 has undergone continuous monitoring with *Swift*. The AGN has exhibited significant UV and X-ray variability while remaining in a moderately low X-ray flux state. A deep 200 ks pointed *XMM–Newton* observation in 2009 attempted to catch the AGN in a minimum in order to study the properties of the photoionized gas observed in the 2007 low state; however, the AGN was instead caught in a transition as it brightened to an intermediate flux level (Grupe et al. 2012, hereafter G12). Interestingly, while the emitting gas is less evident in this intermediate state due to the higher continuum flux compared to the 2007 low state, a warm absorber is now clearly detected (G12; Longinotti et al., submitted to A&A, hereafter L12). Based on their analysis of the reflection grating spectrometer (RGS) data, L12 describe the warm absorber as a combination of three different zones with distinct temperatures and ionization parameters. However, the RGS analysis shows that the ionized gas does not produce the variability observed during this intermediate flux state. The curvature in the X-ray spectrum again could be described by partial covering prompting the suggestion that clouds of absorbing material have been entering the line of sight since 2007 and variations in covering fraction are responsible for the recent low state and variability exhibited by Mrk 335 (G12). Grupe et al. (2008) point to Tanaka, Boller & Gallo (2005) for a partial covering explanation of Mrk 335 in the high-flux state when the covering fraction would have been low.

If the recent diminished flux is due to increased photoelectric absorption from additional partial covering, then it should be accompanied by increased emission in the narrow Fe Kα line (e.g. Reynolds et al. 2009). G12 find that within uncertainties the Fe Kα flux in Mrk 335 is identical in the intermediate- and low-flux states, both of which are comparable to (perhaps even lower than) the Fe Kα flux reported by Grupe et al. (2008) in the high-flux state. In addition, one may expect to find markers of absorption in the UV. There is some indication of absorption in a recent *Hubble Space Telescope (HST)–COS* spectrum of Mrk 335 (L12). However, if and how this is linked to any absorption in the X-ray is difficult to establish since the UV and X-ray observations were not simultaneous.

In this work we test the blurred reflection interpretation for Mrk 335 when the AGN is in an intermediate low-flux state and is significantly modified by a warm absorber, to determine if partial covering is necessary to describe the behaviour of the source in recent years. The observations and data reduction are described in the following section. Spectral modelling is explored in Section 3 and the temporal analysis is described in Section 4. We discuss and summarize our results in Sections 5 and 6, respectively.

2 OBSERVATIONS AND DATA REDUCTION

Mrk 335 has been observed with *XMM–Newton* (Jansen et al. 2001) on five occasions between 2000 and 2009. In this work we report on the long 200 ks observation spread over two consecutive orbits (revolutions 1741 and 1742) in 2009. During the observations the EPIC pn detector (Strüder et al. 2001) was operated in large-window mode and with the thin filter in place. The MOS (MOS1 and MOS2; Turner et al. 2001) cameras were operated in full-frame mode and with the medium filter. RGS1 and RGS2 (den Herder et al. 2001) also collected data during these observations, as did the Optical Monitor (OM; Mason et al. 2001). The OM data have been presented in G12 and will not be reanalysed in this work. These data will be discussed as needed. The RGS analysis is the subject of an in-depth

study of the warm absorber (L12). We will incorporate the results of L12 in this work, but we will not reanalyse the RGS data here.

The *XMM–Newton* Observation Data Files (ODFs) from each observation were processed to produce calibrated event lists using the *XMM–Newton* Science Analysis System (SAS v11.0.0). Unwanted hot, dead or flickering pixels were removed as were events due to electronic noise. Event energies were corrected for charge-transfer inefficiencies. Light curves were extracted from these event lists to search for periods of high background flaring and such periods have been neglected. Pile-up was negligible during the observations. The background photons were extracted from an off-source region on the same CCD. Single and double events were selected for the pn detector, and single–quadruple events were selected for the MOS. EPIC response matrices were generated using the SAS tasks ARFGEN and RMFGEN. The MOS and pn data at each epoch were compared for consistency and determined to be in agreement within known uncertainties (Guainazzi 2010) as was the case in G12. For simplicity we will only present the pn data at each epoch. The total amount of good exposure for the pn during revolutions 1741 and 1742 is 96.4 and 70.0 ks, respectively.

The *XMM–Newton* X-ray spectra were grouped such that each bin contained at least 30 counts. Spectral fitting was performed using XSPEC v12.7.1 (Arnaud 1996). All parameters are reported in the rest frame of the source unless specified otherwise. Figures remain in the observed frame and are binned for display purposes only. Unless stated otherwise, the black, open symbols identify data from revolution 1741, and the filled, red squares represent data from orbit 1742. The quoted errors on the model parameters correspond to a 90 per cent confidence level for one interesting parameter (i.e. a $\Delta\chi^2 = 2.7$ criterion). A value for the Galactic column density towards Mrk 335 of 3.56×10^{20} cm^{-2} (Kalberla et al. 2005) is adopted in all of the spectral fits and abundances are from Anders & Grevesse (1989). Luminosities are calculated using a Hubble constant of $H_0 = 70$ km s^{-1} Mpc^{-1} and a standard flat cosmology with $\Omega_M = 0.3$ and $\Omega_\Lambda = 0.7$.

3 SPECTRAL MODELLING

3.1 The high-energy spectral region

The 2.5–10 keV band in Mrk 335 typically displays curvature both in the high- and low-flux states that can be attributed to blurred reflection (e.g. O'Neill et al. 2007; Grupe et al. 2008; Larsson et al. 2008) or partial covering (e.g. Grupe et al. 2008; G12). Narrow features have also been detected. A narrow $\sim$6.4 keV emission line arising from Fe Kα is regularly observed, while narrow emission features from a highly ionized plasma (Fe XXVI Ly-α, O'Neill et al. 2007) or absorption features attributed to relativistic inflows (Longinotti et al. 2007) are transient.

The 2.5–10 keV spectrum from each epoch was fitted with a power law and a second component to mimic distant reflection. For the distant reflector we consider two models, pexmon (Nandra et al. 2007) and reflionx (Ross & Fabian 2005). Both models self-consistently include Fe Kα, the Compton shoulder and Compton hump. In addition, pexmon includes Fe Kβ and Ni Kα emission. However, pexmon is for reflection off neutral material and does not consider the features that arise below the iron-K band. For reflionx the material is also considered nearly neutral as the ionization parameter ($\xi = 4\pi F_x/n$, where F_x is the incident flux and n is the density of the gas) was set to 1 erg cm s^{-1} (the lowest allowed by the model). Iron abundance is also fixed to the solar value. While there is evidence that the inner accretion disc can show super-solar
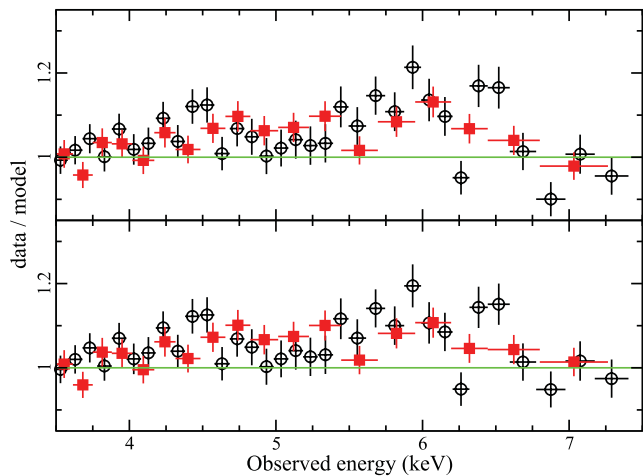
Figure 1. The 2.5–10 keV spectrum is fitted at each epoch with slightly different models for the distant reflector. Top panel: residuals (data/model) remaining in the 3.5–7.5 keV band after fitting the spectra with a power-law plus `pexmon` model. Lower panel: same as above, but using `reflionx` to model the narrow Fe Kα emission line. In both figures the black open circles correspond to the data from revolution 1741 and the filled, red squares are data from revolution 1742. This colour/symbol convention is used throughout the paper unless stated otherwise.

Figure 2. Top panel: the average spectrum in revolution 1741 (black circles) and revolution 1742 (red squares). Lower panel: the ratio of the difference spectrum (rev. 1742 – rev. 1741) fitted with an absorbed power law (Γ ≈ 2.5) between 2 and 10 keV and extrapolated to lower energies. As seen in the top panel the variability is dominated below 1.5 keV.

iron abundances (e.g. Fabian et al. 2009; Reynolds et al. 2012) it is not obvious that this characteristic extends to the distant reflector. However, we note that Walton et al. (2012a) were able to model the *Suzaku* spectrum of Mrk 335 when they allowed the distant reflector (torus) and the inner accretion disc to share common abundances.

Statistically the models fit reasonably well (χ^2_ν/dof = 1.03/1507 and 1.01/1508 for `pexmon` and `reflionx`, respectively), but both models show excess in the residuals between 3.5 and 7.5 keV (Fig. 1). G12 interpreted this excess as evidence for partial covering; we examine this in terms of blurred, ionized reflection from the inner accretion disc. Adding a single Laor profile to both models improved the fits ($\chi^2_\nu \lesssim 1.0$) and residuals significantly in both cases. The equivalent width of the line is $EW \sim 400$ eV in both models. The fitted line parameters are the energy ($E \approx 6.4$ keV), disc emissivity index ($q \approx 4$–8), inner disc radius ($R_{\rm in} \approx 1.3$–5 $r_{\rm g}$, [$r_{\rm g} = GM/c^2$]) and disc inclination ($i \approx 30$–65°). We do not examine these parameters in detail at this point as they will serve as initial values for more realistic models in the remaining analysis.

3.2 The mean 0.3–12 keV spectrum

As seen in Fig. 2, the average spectrum undergoes significant changes between revolution 1741 and 1742. The difference between the two spectra (i.e. rev. 1742 – rev. 1741) fitted with an absorbed power law (Γ ≈ 2.5) between 2 and 10 keV and extrapolated to lower energies is shown in the lower panel of Fig. 2 . The changes are substantial below ∼1.5 keV, but there is also indication for variability above 2 keV. For this reason we will treat the data from each epoch separately when examining the spectra.

There is a significant warm absorber present at both epochs, which is clearly seen in the RGS spectra, and is the subject of other work (L12). This is the first time that a warm absorber has been unambiguously observed in Mrk 335. L12 identified three distinct ionized components, all outflowing at high velocity (∼5000 km s^{-1}). However, since L12 determined that the warm absorber itself is not variable during these observations, it cannot be the warm absorber
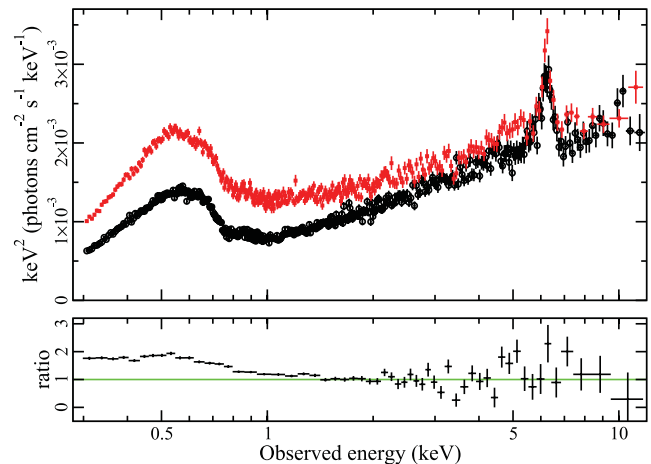
that is responsible for the changes seen in Fig. 2. To remain consistent with the RGS analysis, we constructed XSTAR (Kallman & Bautista 2001) grids that are comparable with the three warm absorbers found in L12. These components are included in our spectral fitting and are linked between the epochs.

The neutral reflector originating from distant matter is modelled with `reflionx` rather than `pexmon` since it offers a more complete treatment of the reflection at low energies. This component should not be confused with the reflection from the inner disc as it is not subject to any blurring effects. The ionization parameter of this distant reflector is fixed at $\xi = 1.0$ erg cm s^{-1} (i.e. the lowest value permitted by the model) and the iron abundance is fixed to solar. The photon index of the ionizing power law is fixed to the canonical value of Γ = 1.9 (Nandra & Pounds 1994). It is not clear if this assumption is accurate as the photon index is clearly variable in Mrk 335 (e.g. $1.5 \lesssim \Gamma \lesssim 2.3$ have been reported). It is also not obvious that the torus would be illuminated by the same power law that is seen by the observer since the line of sight through the corona, and hence the optical depth, is likely different from each perspective. The normalization of this component is linked at both epochs.

In the 2007 low flux state observation, Grupe et al. (2008) and Longinotti et al. (2008) identified narrow emission features attributed to a distant photoionized plasma. The CCD spectra were fitted with a MEKAL model to account for this emission (Grupe et al. 2008), but the fitting was rather ad hoc and did not account for some of the strongest features in the spectrum (e.g. a 0.89 keV emission feature and the narrow Fe Kα emission line). Such emission is not prominent in the 2009 RGS data (L12) and this could simply be a matter of the higher continuum flux overwhelming the hot, diffuse plasma. We do not specifically consider the reasonable assumption that a constant MEKAL component (e.g. fixed to the 2007 values) is present in these 2009 data, but we note that the distant reflector modelled by the unblurred `reflionx` component can similarly describe this emission. The 0.5–10 keV flux of the MEKAL component in the low-flux spectrum was ∼2.2 × 10^{-13} erg cm^{-2} s^{-1} , comparable to the flux of the distant reflector used in these models (see Table 1).

After fitting the three-phase warm absorber to the RGS data, L12 attributed the remaining residuals between about 0.49 and 0.65 keV

Table 1. The best-fitting model parameters for the multi-epoch spectral modelling of Mrk 335. The model components and model parameters are listed in columns 1 and 2, respectively. Columns 3 and 4 list the parameter values during revolutions 1741 and 1742, respectively. The inner (R_{in}) and outer (R_{out}) disc radii are given in units of gravitational radii ($1\,r_g = GM/c^2$). The reflection fraction ($\mathcal{R}$) is approximated as the ratio of the reflected flux over the power-law flux in the 20–50 keV band. Values that are linked between epochs appear only in column 3. The superscript f identifies parameters that are fixed and the superscript p indicates values that are pegged at a limit. Fluxes are corrected for Galactic absorption and are reported in units of $\mathrm{erg\,cm^{-2}\,s^{-1}}$.

(1) Model component	(2) Model parameter	(3) 1741	(4) 1742
Warm absorber 1	$N_H\ (\times 10^{21})$	$2.92^{+0.89}_{-0.62}$	
	$\log\xi\ (\mathrm{erg\,cm\,s^{-1}})$	$0.98^{+0.05}_{-0.19}$	
Warm absorber 2	$N_H\ (\times 10^{21})$	$1.24^{+0.86}_{-0.54}$	
	$\log\xi\ (\mathrm{erg\,cm\,s^{-1}})$	1.89 ± 0.08	
Warm absorber 3	$N_H\ (\times 10^{21})$	$11.8^{+2.9}_{-5.5}$	
	$\log\xi\ (\mathrm{erg\,cm\,s^{-1}})$	2.81 ± 0.05	
Power law	Γ	1.83 ± 0.01	1.98 ± 0.02
	$\log F_{0.5-10\,keV}$	-11.27 ± 0.02	-11.24 ± 0.04
Blurring	q_{in}	$7.03^{+1.24}_{-0.85}$	
	$R_{in}\ (r_g)$	$1.38^{+0.07}_{-0.145}{}^{p}$	
	$R_{out}\ (r_g)$	400^{f}	
	$R_b\ (r_g)$	$5.78^{+1.94}_{-1.16}$	
	q_{out}	3^{f}	
	$i\ (°)$	51^{+10}_{-13}	
Reflection	$\xi\ (\mathrm{erg\,cm\,s^{-1}})$	200^{+2}_{-23}	244^{+27}_{-15}
	A_{Fe} (Fe/solar)	1.67 ± 0.18	
	$\log F_{0.5-10\,keV}$	-11.32 ± 0.02	-11.06 ± 0.02
	$\mathcal{R}$	1.79	2.05
Distant reflector	$\xi\ (\mathrm{erg\,cm\,s^{-1}})$	1.0^{f}	
	A_{Fe} (Fe/solar)	1.0^{f}	
	Γ	1.9^{f}	
	$\log F_{0.5-10\,keV}$	$-12.24^{+0.03}_{-0.06}$	
	$\mathcal{R}$	1.13	1.59
Fit quality	χ^2_ν/dof	$1.06/2379$	

to intrinsically narrow emission corresponding to O VIII and N VII Lyα, as well as the O VII triplet. Adding Gaussian profiles with fixed energies and widths, but free normalizations, to the CCD data did not result in any detection of these features. For each line, the measured equivalent width was $EW < 1$ eV. Including the Gaussian features with all parameters fixed to the RGS measured values generated an entirely comparable fit to the one presented in Table 1.

The broad-band continuum is described with a power-law plus reflection from the accretion disc. It is then modified by a three-zone warm absorber and a distant neutral absorber. The reflection component is blurred for dynamical effects in the disc close to the black hole using `kdblur2` with a broken power-law emissivity profile. The objective was to obtain a self-consistent model that described both observations. Despite the significant variability the observations were separated by only $\sim$42 ks; consequently, we were selective in what we allowed to vary between the observations. In addition to the distant reflector, the inclination (i), iron abundance (A_{Fe}), inner (R_{in}) and outer (R_{out}) disc radius were linked between the observations. Initial fits were conducted with the inner emissivity profile (q_{in}) and the break radius (R_b) free to vary at each

epoch. The outer emissivity profile (q_{out}) was fixed to 3 as would be expected in the case for illumination of the disc from a distant source. Finding no significant differences in the values of R_b and q_{in} during revolutions 1741 and 1742, the parameters were also linked in subsequent fits. The best-fitting model reported here allows only the photon index and normalization of the power-law component, and the ionization and normalization of the reflector to vary at each epoch.

The model adequately fits the data ($\chi^2_\nu/\mathrm{dof} = 1.06/2379$). The model parameters and fit are shown in Table 1 and Fig. 3, respectively. The reflection model makes specific predictions of the spectral appearance above 10 keV. While simultaneous observations above 10 keV do not exist, the average *Swift* BAT spectrum is available for comparison (Fig. 4). The *Swift* data agree well with the blurred reflection spectral model.

The differences between the two epoch require changes in the normalizations as well as the shape of the reflection and power-law components. In contrast to typical observations the reflection component appears more dominant during revolution 1742 when the AGN is in a higher flux state.
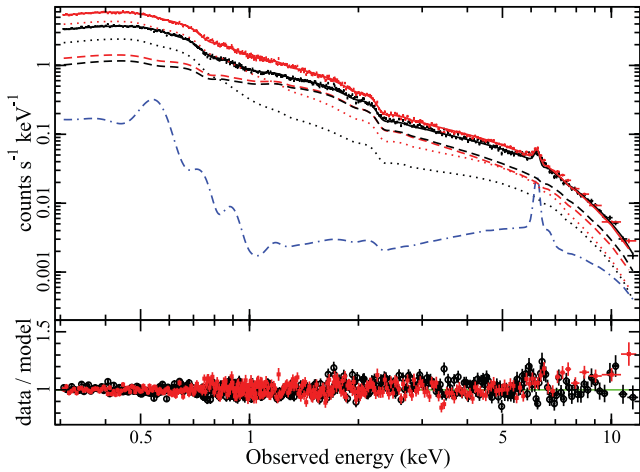
Figure 3. Top panel: the average spectrum in revolution 1741 (black circles) and revolution 1742 (red squares) over the 0.3–12 keV band fitted with the best-fitting model (Table 1). The dotted lines are the blurred reflector and the dashed curves are the intrinsic power law. The distant reflector is common to both spectra and is shown in blue (dashed–dotted curve). Lower panel: the data-to-model ratio resulting from the best-fitting model.
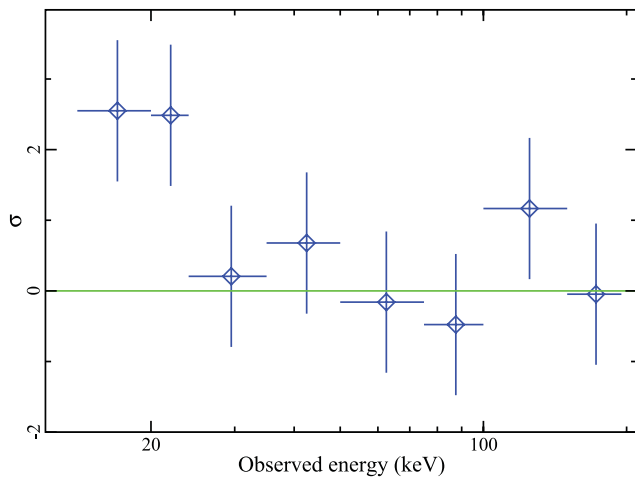

Figure 4. The best-fitting model described in this section is extrapolated to high energies and compared (i.e. not fitted) to the *Swift* BAT data. The residuals are shown in terms of sigma.

3.3 Black hole spin

In accordance with the small inner radius found in the fit (Table 1) a high black hole spin value is expected in Mrk 335. In order to estimate the black hole spin we conservatively concentrate efforts on the high-energy spectrum above 2.5 keV. When fitting the broad-band spectrum the spin value is often highly dependent on the interpretation and modelling of the smooth soft excess where the statistics are highest, and as we know from L12, this region is significantly modified by the three-zone warm absorber.

We begin with the power-law plus distant reflector model described in Section 3.1. To this we add a reflector that is blurred using `kerrconv` (Brenneman & Reynolds 2006; instead of `kdblur2`), which includes the black hole spin as a model parameter. As in the broad-band spectral analysis, all model parameters are tied except for the power-law photon index and normalization, and the blurred reflector ionization and normalization. A good fit to the 2.5–10 keV data is found ($\chi^2_\nu/\mathrm{dof} = 0.96/1307$) with all model parameters in
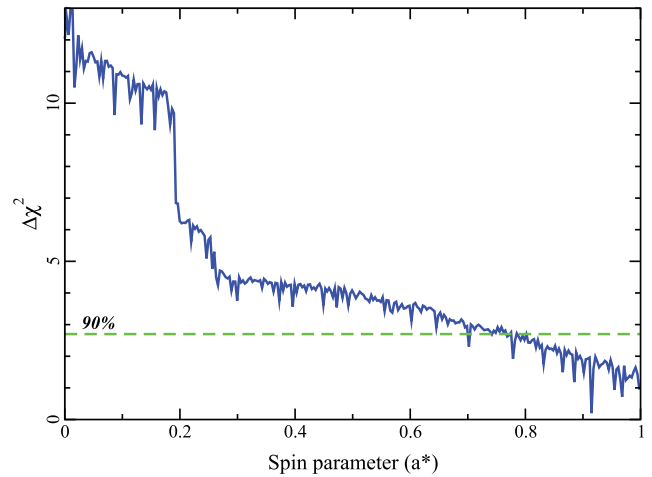

Figure 5. The quality of the fit is tested against the black hole spin parameter showing that extremely low spins are discriminated against. The minimum in $\Delta\chi^2$ is at $a \approx 0.9$. The green, dashed line marks the 90 per cent confidence level.

agreement with the broad-band results in Table 1 (albeit with larger uncertainties).

In order to estimate the uncertainty on the measured spin we examine the variation in the quality of the fit associated with the changes in the spin parameter (Fig. 5). Relatively high spin values are preferred by the fit ($0.76 < a < 0.998$) at 90 per cent confidence. Very low spin values ($a < 0.2$) are rejected at the 3σ level. The spin parameter measured from these data of Mrk 335 in a warm absorber dominated, intermediate flux state is in agreement with that measured by Walton et al. (2012a) using the *Suzaku* XIS and PIN spectra of Mrk 335 in an unabsorbed, high-flux state ($a = 0.8 \pm 0.1$), and commensurate with the small inner disc radius found by Crummy et al. (2006).

4 X-RAY VARIABILITY

G12 reported significant flux and spectral variability over the intermediate flux level observations examined here (see their fig. 5). We attempt to describe the variability in Mrk 335 based on the blurred reflection model presented in Section 3.2. As noted in Section 3.2, variability is seen in power-law normalization and shape as well as in the ionization and flux of the reflector. Here we examine how the model can account for the spectral variability as a function of time and flux level.

4.1 Flux-resolved spectroscopy

Spectra are created in four flux bins during revolution 1741 and three flux bins during revolution 1742, as defined in Fig. 6. The high-, medium- and low-flux states are defined identically in 1741 and 1742. The extra-low-flux state (i.e. xlow) is unique to 1741 as the AGN brightness does not dip to this level during 1742. In Fig. 7, we plot the spectra from each flux state against a power law ($\Gamma = 2$) absorbed by Galactic column density. Despite the comparable brightness the flux-resolved spectra differ notably between 1741 and 1742.

The various flux states during each orbit were fitted simultaneously using the best-fitting model from Section 3.2 as the starting condition. The warm absorber and distant reflector parameters were fixed to their average values. Initially, the blurring parameters q_{in}
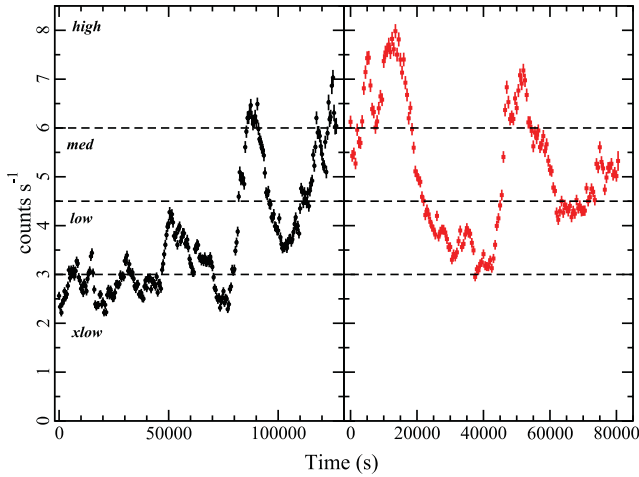
Figure 6. The 0.2–12 keV pn light curve in 500 s bins from revolutions 1741 (left) and 1742 (right). Zero second marks the start of each observation. The dashed lines delineate the various flux levels examined in Section 4.1. The high, medium and low state are defined with count rates of >6, 4.5–6.0 and 3–4.5 counts s^{-1}. Revolution 1741 also is separated into an extra low state (<3 counts s^{-1}).
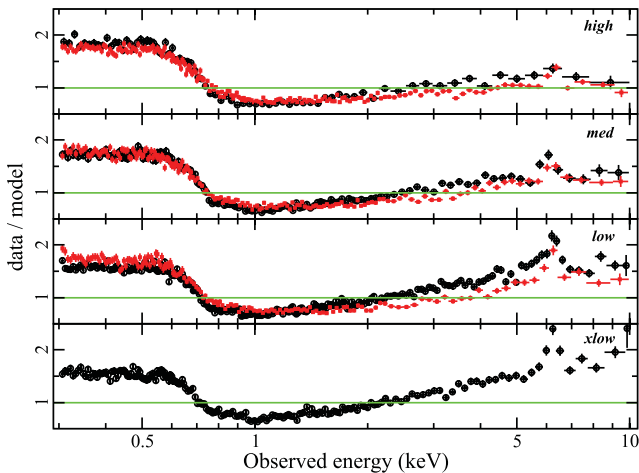

Figure 7. Spectra extracted from the flux levels defined in Fig. 6 are compared to an absorbed power law with $\Gamma = 2$. Despite the comparable flux there exist differences between the flux-resolved spectra from the two observations.

and R_b were free, but since neither demonstrated noticeable variability they were fixed to their average values as well. The only free parameters were the photon index of the power-law continuum, ionization parameter of the reflector and the normalization of both components.

The spectral variations are well fitted by allowing only these parameters to vary (χ^2_ν/dof = 1.02/3525 for revolution 1741 and χ^2_ν/dof = 1.01/2502 for revolution 1742). The residuals from the fits are shown in Fig. 8. Some trends resulting from fitting the flux-resolved spectra are shown in Fig. 9. As found when modelling the average spectra, the ionization parameter of the blurred reflector is distinctly higher during revolution 1742. This is seen in the flux-resolved spectra as well; however, there does not appear to be a gradual change with increasing flux that might be expected (Fig. 9a). We note that the telescope does not collect data for ~40 ks between revolution 1741 and 1742, which makes it difficult to draw
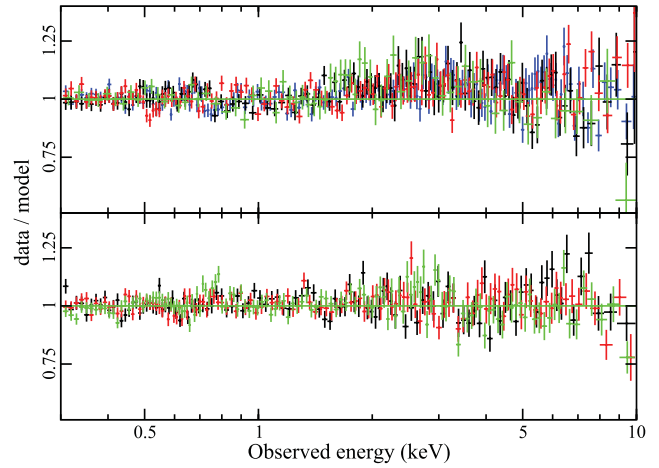

Figure 8. The ratio (data/model) from fitting the various flux states defined in Fig. 6 with a model in which the reflection and power-law component are allowed to vary (see the text for details). Data from 1741 and 1742 are shown in the top and bottom panel, respectively. The black, red and green data points mark the low-, medium- and high-flux states. The blue data points in the top panel identify the extra-low-flux state during 1741.

strong conclusions as to when the change in the ionization parameter occurs.

Other parameters do appear to exhibit predicable behaviour. The power-law slope is seen to steepen with increasing flux (Fig. 9b). The power-law flux and reflected flux are also correlated, which would occur if the primary emitter brightens intrinsically and illuminates the disc more (Fig. 9c). The reflection fraction ($\mathcal{R}$), which is taken to be the ratio between the reflected and power-law flux between 20 and 50 keV, is also correlated with the reflected flux (Fig. 9d). We note that the relationship between the two parameters is different at each epoch, which could be due to the simultaneous changes in the power-law photon indices.

4.2 Time-resolved spectroscopy

In order to investigate the model variability over time, spectra were created using 10 ks intervals of data resulting in 12 spectra in 1741 and 7 spectra in 1742. Each spectrum was modelled by allowing only the power-law normalization and slope to vary as well as the reflector normalization and ionization. Figs 10 and 11 portray our findings.

The average ionization of the reflector is different at each epochs, but as we see in the top panels of Fig. 10, the ionization parameter does not vary with the short time-scale changes in the reflected flux (lower panels of Fig. 10). Similar behaviour was seen in the flux-resolved spectra (Fig. 9a).

The flux of the reflector (lower panels of Fig. 10) is variable over the course of the observations, as is the flux and the photon index of the power-law component (Fig. 11). Of interest is that during the first 70 ks of 1741 the flux of the reflection component is approximately constant (Fig. 10, lower-left panel) as is the shape and flux of the power-law component (Fig. 11, left). In general, the reflected flux appears to be well correlated with changes in the power-law component. The specific correlation between the photon index and the reflected flux is shown in Fig. 12 and exists in both the time-resolved and flux-resolved spectra. Since the reflection fraction ($\mathcal{R}$) increases with reflected flux (Fig. 9d), the observed trend in Fig. 12 between the shape of the intrinsic power law illuminating
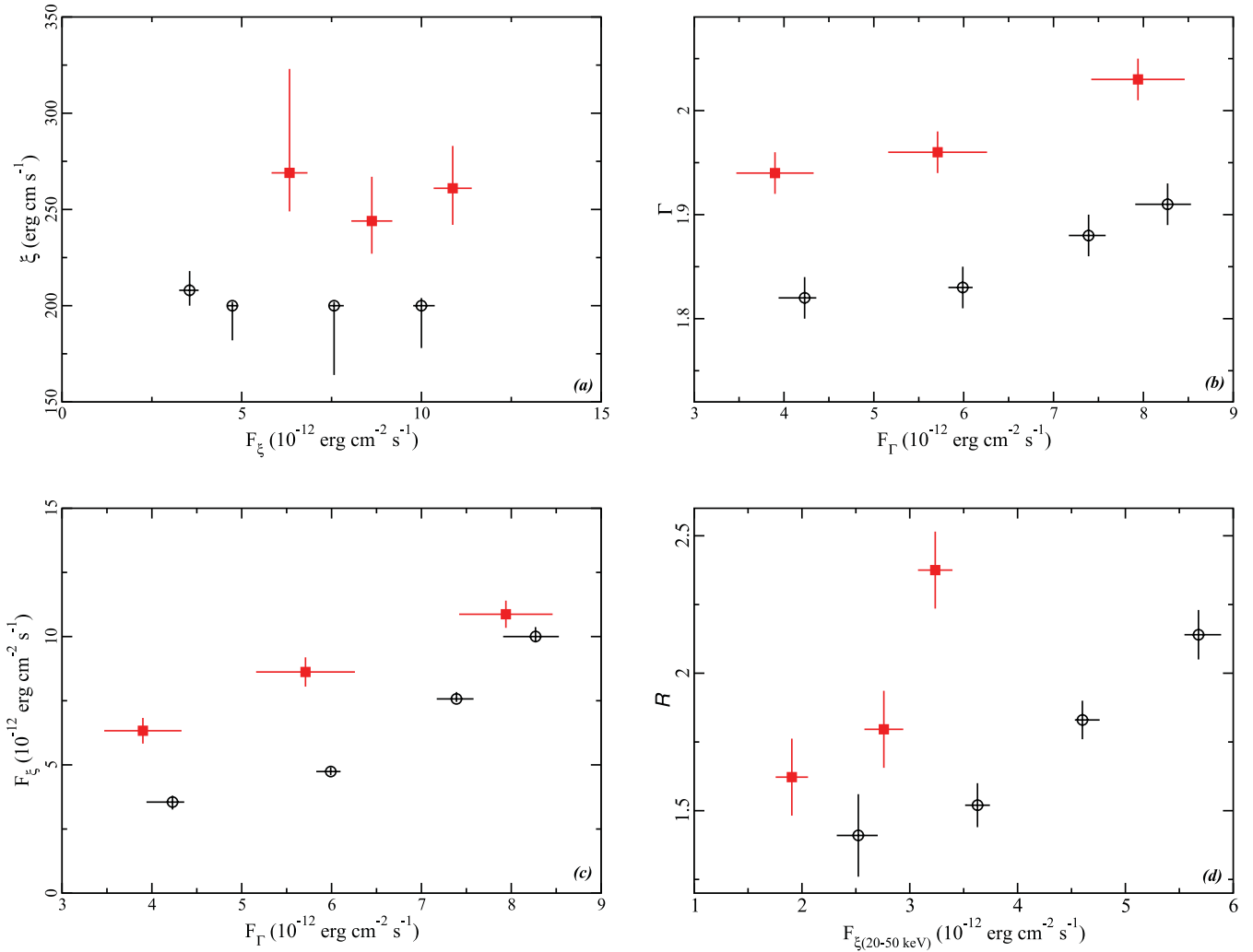
Figure 9. The variability of various parameters in different flux states during 1741 (black open circles) and 1742 (red filled squares). (a) The ionization parameter of the reflector as a function of the reflected flux (F_ξ) in the 0.3–10 keV band. (b) The power-law photon index as a function of the power-law flux (F_Γ) in the 0.3–10 keV band. (c) The reflected flux is plotted against the powerlaw flux. (d) The reflection fraction, between 20 and 50 keV, is compared to the reflected flux in the same band.

Figure 10. The variability of the reflection component is tracked over the entire observation by fitting 10 ks resolved spectra during revolutions 1741 (left-hand panel) and 1742 (right-hand panel). The flux (lower panels) and ionization parameters (upper panels) are compared to the average values (solid lines). The ionization parameter appears constant during both observations, but the flux is variable. The reflected flux during revolution 1741 (lower-left panel) is compared to the average during the first 70 ks of the observation (dashed line). The flux appears constant during this segment of the observation.
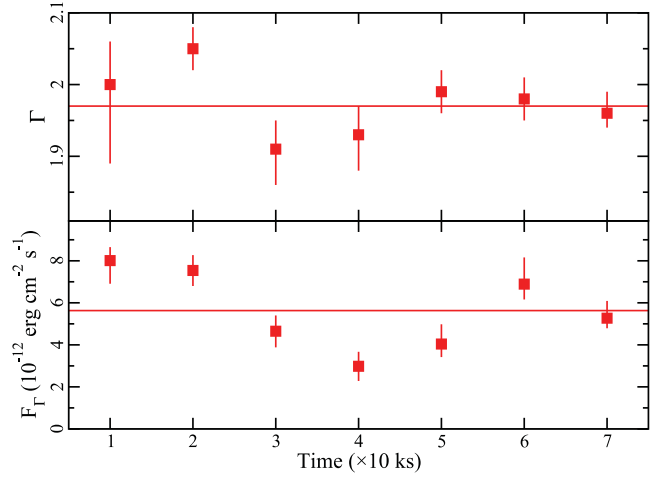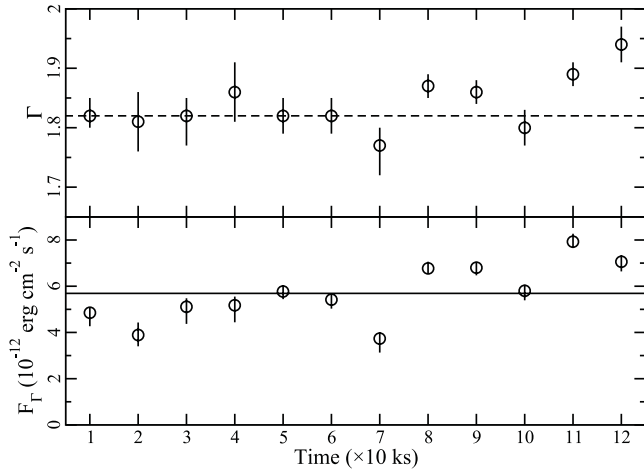
Figure 11. The variability of the power-law component is tracked over the entire observation by fitting 10 ks resolved spectra during revolutions 1741 (left-hand panel) and 1742 (right-hand panel). The flux (lower panels) and photon index (upper panels) are compared to the average values (solid lines) and both parameters appear variable. The photon index during revolution 1741 (upper-left panel) is compared to the average during the first 70 ks of the observation (dashed line). The photon index appears constant during this segment of the observation.
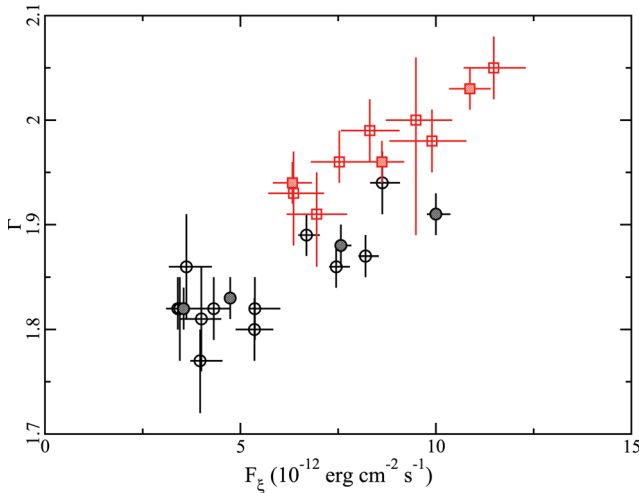
Figure 12. The variations of the power-law photon index plotted against the variations in the reflected flux. The relation between the two parameters is seen in the time-resolved spectra (open symbols) as well as in the flux-resolved spectra (shaded symbols).
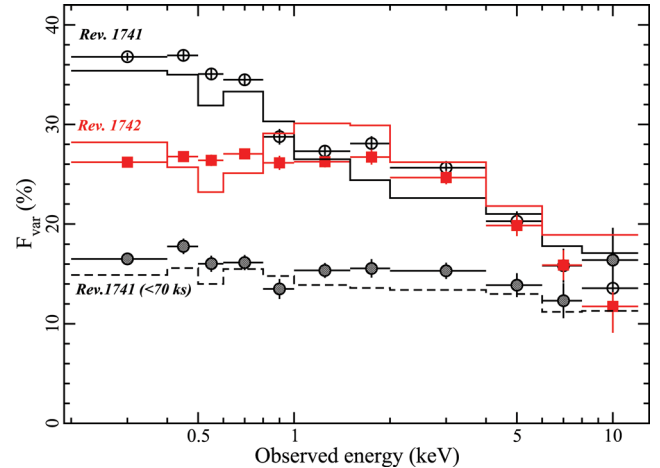
Figure 13. The fractional variability as a function of energy is calculated for observations 1741 (black open circles) and 1742 (red filled squares), as well as for the first 70 ks of observation 1741 (black, shaded circles). The models described in Section 4.2 are overplotted and show reasonable agreement with the data.

the accretion disc and the reflected flux is expected (see e.g. fig. 4 of Ross & Fabian 2005).

The variability behaviour also describes the appearance of the fractional variability (F_{var}) spectrum of Mrk 335 at each epoch (Fig. 13). The F_{var} in each energy band is calculated with light curves in 500 s bins following Edelson et al. (2002) and uncertainties are estimated following Ponti et al. (2004). There is clearly a difference below ~1 keV in the F_{var} spectra between the two epochs with 1741 showing larger variations at lower energies. The F_{var} spectrum is also calculated for only the first 70 ks of revolution 1741 (shaded, black circles), showing much smaller variations over this reduced period. Each F_{var} spectrum can be reasonably depicted by the variations found in Figs 10 and 11. The first 70 ks of 1741 are described by variations in only the power-law normalization, while to describe the average F_{var} in 1741 (black open circles) variability in the remaining ~50 ks requires additional changes in the power-

law slope and reflector normalization. The variability in 1742 also requires changes in the power-law shape and normalization and in the reflector normalization.

5 DISCUSSION

Blurred reflection is expected when the inner accretion disc extends down towards the radius of marginal stability around a black hole. Many of the concerns raised over blurred reflection are now coming into focus with recent X-ray data. The discovery of broadened Fe Lα and short lags (e.g. Fabian et al. 2009; Zoghbi et al. 2010) suggests that the soft excess in AGN is due to reflection and that it arises from reprocessing of the primary continuum. The broad Fe Kα line is also seen in black hole binaries (BHB) (e.g. Miller et al. 2009) showing that reflection is ubiquitous in black hole systems. The similarities in the Fe Kα profile seen in AGN and BHB (Walton

et al. 2012b) argue strongly in favour of the reflection interpretation. Moreover, the evidence for blurred reflection is not limited to unique systems or specific lines of sight. Evidence of reflection is seen in most systems where there is a direct view of the central regions (e.g. Crummy et al. 2006; De Marco et al. 2011; Walton et al. 2012a; Zoghbi et al. 2012).

The *XMM–Newton* observations of Mrk 335 analysed here provide a view of the AGN that is distinct from previous observations, First, by the presence of a complex warm absorber (analysed by L12) and secondly through the significant and rapid spectral variability. Over the course of the 200 ks observation the source becomes notably softer as it brightens. When examining the light curve from the long-term *Swift* monitoring campaign (G12), we find that these *XMM–Newton* observations catch Mrk 335 in rapid transition from a low-flux to a high-flux state (G12). The X-ray continuum is well described with a primary power-law emitter and blurred reflection from the inner region of the accretion disc around a rapidly spinning black hole. The blurred reflection model also accurately describes the variability assuming that the continuum components are allowed to vary. Specifically, the photon index and power-law normalization as well as the reflector ionization and normalization are changing.

Though the behaviour is complex, the variability in the parameters is largely consistent with what is expected. The overall changes appear to be driven by the pivoting of the power-law component (i.e. the primary emitter). The power-law flux increases as the spectrum steepens, in line with expectations (e.g. Haardt, Maraschi & Ghiselini 1997). Assuming that the distance between the primary emitter and the disc does not change, the flux and ionization of the disc will increase accordingly, as is seen.

The changes in the power-law photon index occur very rapidly. During the first 70 ks of the observation Mrk 335 did not exhibit any notable spectral variability. The apparent change in the photon index, specifically steepening from $\Gamma \approx 1.83$ to $\Gamma \approx 1.98$, occurs over $\sim$50 ks in the rest frame. A scenario in which the primary emitter could be moving at mildly relativistic velocities with respect to the disc (e.g. Reynolds & Fabian 1997; Beloborodov 1999) could be invoked to drive the changes in Γ. This interpretation has been advocated for other AGN and NLS1s (e.g. Gallo et al. 2007, 2011; Miniutti et al. 2010). However, while light bending is certainly prominent, the rather constant emissivity profile and break radius obtained in our spectral fitting of Mrk 335 suggest that the blurring parameters do not change as would be expected if the primary source varies its distance from the disc.

Fabian et al. (2012) suggest a double power-law continuum to describe the low state X-ray spectrum of Cyg X-1. There they suggest that the steeper component originates at the base of the jet and is responsible for the reflection with the harder component located farther up the jet. This scenario could perhaps be expanded to describe the observations in Mrk 335. One could imagine multiple jet components coming together at the base of a jet located close to the disc, for example a jet 'blob' that does not obtain the escape velocity and falls back downstream towards the base (e.g. Ghiselini et al. 2004). The coming together of two components of differing densities could produce the changes seen in the power law and ultimately in the reflection. Interestingly, a double power-law continuum was suggested for the blurred reflection interpretation of the very low flux state observation of Mrk 335 (Grupe et al. 2008). Mrk 335 is certainly radio-quiet, but not radio silent ($R = L_\nu(\text{5 GHz})/L_\nu(B) \approx 0.25$) so the possibility of some jet emission does exist.

6 CONCLUSIONS

The most recent *XMM–Newton* observations of Mrk 335 catch the AGN in a complex, intermediate flux state. Both the X-ray continuum and timing properties of the NLS1 can be described in a self-consistent manner adopting a blurred reflection model without any need to invoke partial covering. The rapid spectral variability appears to be driven by changes in the spectral shape of the primary emitter that is illuminating the inner accretion disc.

REFERENCES

Anders E., Grevesse N., 1989, Geochim. Cosmochim. Acta, 53, 197
Arnaud K., 1996, in Jacoby G., Barnes J., eds, ASP Conf. Ser. Vol. 101, Astronomical Data Analysis Software and Systems. Astron. Soc. Pac., San Francisco, p. 17
Ballantyne D. R., Iwasawa K., Fabian A. C., 2001, MNRAS, 323, 506
Beloborodov A. M., 1999, MNRAS, 510, 123
Brenneman L. W., Reynolds C. S., 2006, ApJ, 652, 1028
Crummy J., Fabian A., Gallo L., Ross R., 2006, MNRAS, 365, 1067
De Marco B., Ponti G., Cappi M., Dadina M., Uttley P., Cackett E. M., Fabian A. C., Miniutti G., 2011, MNRAS, preprint (arXiv:1201.0196)
den Herder J. W. et al., 2001, A&A, 365, 7
Edelson R., Turner T. J., Pounds K., Vaughan S., Markowitz A., Marshall H., Dobbie P., Warwick R., 2002, ApJ, 568, 610
Fabian A. C. et al., 2009, Nat, 459, 540
Fabian A. C. et al., 2012, MNRAS, 424, 217
Gallo L. C., 2006, MNRAS, 368, 479
Gallo L. C., Brandt W. N., Costantini E., Fabian A. C., 2007, MNRAS, 377, 1375
Gallo L. C., Miniutti G., Miller J. M., Brenneman L. W., Fabian A. C., Guainazzi M., Reynolds C. S., 2011, MNRAS, 411, 607
Ghiselini G., Haardt F., Matt G., 2004, A&A, 413, 535
Grupe D., Komossa S., Gallo L. C., 2007, ApJ, 668, 111
Grupe D. et al., 2008, ApJ, 681, 982
Grupe D., Komossa S., Gallo L. C., Longinotti A. L., Fabian A. C., Pradhan A. K., Gruberbauer M., Xu D., 2012, ApJS, 199, 28 (G12)
Guainazzi M., 2010, XMM–Newton Calibration Documents, CAL-TN-0018
Haardt F., Maraschi L., Ghiselini G., 1997, ApJ, 476, 620
Jansen F. et al., 2001, A&A, 365, L1
Kalberla P. M. W., Burton W. B., Hartmann D., Arnal E. M., Bajaja E., Morras R., Pöppel W. G. L., 2005, A&A, 440, 775
Kallman T., Bautista M., 2001, ApJS, 133, 221
Larsson J., Miniutti G., Fabian A. C., Miller J. M., Reynolds C. S., Ponti G., 2008, MNRAS, 384, 1316
Longinotti A. L., Nucita A., Santos-Lleo M., Guainazzi M., 2008, A&A, 470, 73
Mason K. O. et al., 2001, A&A, 365, 36
Miller J. M., Reynolds C. S., Fabian A. C., Miniutti G., Gallo L. C., 2009, ApJ, 697, 900
Miniutti G., Piconcelli E., Bianchi S., Vignali C., Bozzo E., 2010, MNRAS, 401, 1315
Nandra K., O'Neill P. M., George I. M., Reeves J. N., 2007, MNRAS, 382, 194
Nandra K., Pounds K. A., 1994, MNRAS, 268, 405

O'Neill P. M., Nandra K., Cappi M., Longinotti A. L., Sim S. A., 2007, MNRAS, 381, 94

Ponti G., Cappi M., Dadina M., Malaguti G., 2004, A&A, 417, 451

Pounds K. A., Stanger V. J., Turner T. J., King A. R., Czerny B., 1987, MNRAS, 224, 443

Reynolds C. S., Fabian A. C., 1997, MNRAS, 290, L1

Reynolds C. S., Fabian A. C., Brenneman L. W., Miniutti G., Uttley P., Gallo L. C., 2009, MNRAS, 397, 21

Reynolds C. S., Brenneman L. W., Lohfink A. M., Trippe M. L., Miller J. M., Fabian A. C., Nowak M. A., 2012, ApJ, 755, 88

Ross R. R., Fabian A. C., 2005, MNRAS, 358, 211

Strüder L. et al., 2001, A&A, 365, L18

Tanaka Y., Boller T., Gallo L., 2005, in Merloni A., Nayakshin S., Sunyaev R. A., eds, ESO Conf. Ser., Growing Black Holes: Accretion in a Cosmological Context. Springer-Verlag, Berlin, p. 290

Turner M. J. L. et al., 2001, A&A, 365, 27

Walton D. J., Nardini E., Fabian A. C., Gallo L. C., Reis R. C., 2012a, MNRAS, accepted

Walton D. J., Reis R. C., Cackett E. M., Fabian A. C., Miller J. M., 2012b, MNRAS, 422, 2510

Zoghbi A., Fabian A. C., Uttley P., Miniutti G., Gallo L. C., Reynolds C. S., Miller J. M., Ponti G., 2010, MNRAS, 401, 2419

Zoghbi A., Fabian A. C., Reynolds C. S., Cackett E. M., 2012, MNRAS, 422, 129

This paper has been typeset from a T$_{\rm E}$X/L$^{\rm A}$T$_{\rm E}$X file prepared by the author.